Letter | Editors' Suggestion

Ultrahigh resolution x-ray Thomson scattering measurements at the European X-ray Free Electron Laser

Thomas Gawne,[1,2,*] Zhandos A. Moldabekov,[1,2] Oliver S. Humphries,[3] Karen Appel,[3] Carsten Baehtz,[2] Victorien Bouffetier,[3] Erik Brambrink,[3] Attila Cangi,[1,2] Sebastian Göde,[3] Zuzana Konôpková,[3] Mikako Makita,[3] Mikhail Mishchenko,[3] Motoaki Nakatsutsumi,[3] Kushal Ramakrishna,[1,2] Lisa Randolph,[3] Sebastian Schwalbe,[1,2] Jan Vorberger,[2] Lennart Wollenweber,[3] Ulf Zastrau,[3] Tobias Dornheim,[1,2,†] and Thomas R. Preston[3,‡]

[1]*Center for Advanced Systems Understanding (CASUS), D-02826 Görlitz, Germany*

[2]*Helmholtz-Zentrum Dresden-Rossendorf (HZDR), D-01328 Dresden, Germany*

[3]*European XFEL, D-22869 Schenefeld, Germany*

(Received 4 March 2024; revised 15 May 2024; accepted 20 May 2024; published 12 June 2024)

Using an ultrahigh resolution ($\Delta E \sim 0.1$ eV) setup to measure electronic features in x-ray Thomson scattering (XRTS) experiments at the European XFEL in Germany, we have studied the collective plasmon excitation in aluminium at ambient conditions, which we can measure very accurately even at low momentum transfers. As a result, we can resolve previously reported discrepancies between *ab initio* time-dependent density functional theory simulations and experimental observations. The demonstrated capability for high-resolution XRTS measurements will be a game changer for the diagnosis of experiments with matter under extreme densities, temperatures, and pressures, and unlock the full potential of state-of-the-art x-ray free electron laser (XFEL) facilities to study planetary interior conditions, to understand inertial confinement fusion applications, and for material science and discovery.

DOI: 10.1103/PhysRevB.109.L241112

The x-ray Thomson scattering (XRTS) technique [1] has emerged as a powerful method of diagnosing matter. By probing the electronic dynamic structure factor $S_{ee}(q, E)$, where q and E are the change in the momentum and energy of the scattered photon, it is capable of giving detailed insights into the microphysics of the probed sample [2–4]. This capability is particularly important for experiments with matter under extreme densities, temperatures, and pressures [2,5,6], as they occur, e.g., in astrophysical objects [7–9], inertial confinement fusion applications [10,11], and for material science and materials discovery [12–14]. Here, the combination of the extreme conditions with the highly transient nature of the generated extreme states in the laboratory [15] renders the unambiguous diagnosis of plasma conditions challenging.

Since the first observation of plasmons in warm dense beryllium [16], a number of major developments have helped to establish XRTS as a reliable method for the study of materials over a vast range of densities and temperatures. This includes the demonstration of ultrabright seeded x-ray free-electron laser (XFEL) beams [17], the utilization of XRTS for the detection and quantification of miscibility [18], and the resolution of ion acoustic modes in single-crystal diamond [19].

The measured XRTS intensity is given by [1,2,20]

$$I(q, E_s) = S_{ee}(q, E_0 - E_s) \circledast R(E_s), \tag{1}$$

i.e., as a convolution of $S_{ee}(q, E)$ with the combined source-and-instrument function $R(E_s)$, where E_0 and E_s denote the beam energy and the energy of the scattered photon. In practice, deconvolving Eq. (1) is generally numerically unstable; the width of $R(E_s)$ thus limits the capability of XRTS to resolve electronic features such as sharp plasmon excitations. This strongly hampers the model-free diagnosis of parameters, such as the temperature [20,21], that are important for equation-of-state measurements [22,23], and poses a serious obstacle for the benchmarking of theoretical models against experimental observations [24,25].

In this Letter, we present measurements of the plasmon in Al with an unprecedented resolution of $\Delta E \sim 0.1$ eV that allows us to resolve electronic features from XRTS measurements and reconcile discrepancies in modeling. Our measurements of Al at ambient conditions, made with a new setup at the European XFEL in Germany [27], using a seeded and monochromated beam, are in excellent agreement with previous electron energy loss spectroscopy (EELS) measurements [28,29]. In addition, the high resolution of our results allows us to unambiguously benchmark time-dependent density functional theory (TDDFT) [30] calculations, and to resolve discrepancies reported in previous works [24,25].

This new capability will be of paramount importance for XRTS diagnostics: first and foremost, it allows for the model-free interpretation of the measured spectra even for

*t.gawne@hzdr.de
†t.dornheim@hzdr.de
‡thomas.preston@xfel.eu

Published by the American Physical Society under the terms of the Creative Commons Attribution 4.0 International license. Further distribution of this work must maintain attribution to the author(s) and the published article's title, journal citation, and DOI.

comparably moderate temperatures of $T \sim 1\,\text{eV}$, whereas previous experimental setups were limited to $T > 10\,\text{eV}$ [20,21]. This will unlock the full potential of modern XFEL facilities for material science and discovery [12–14], for the characterization of the initial phase of the compression path of the fuel capsule in laser fusion experiments, and for the study of planetary interior conditions [7]. We note that, despite its comparable resolution, EELS generally cannot be used to diagnose experiments in this regime due to its stringent requirements for thin targets and long measurement times [31]. Furthermore, to temporally resolve XRTS in WDM requires a femtosecond x-ray free electron laser such as that at the European XFEL. Due to the short femtosecond timescales of FELs we can isochorically heat with the FEL beam to temperatures in the WDM matter regime [32]. If defocussed, the FEL can also be used as a fs probe in the event of another driver being used in a pump-probe setup, enabling studies of highly transient states which cannot be performed elsewhere.

In addition, we have demonstrated the capability of our XRTS setup to produce rigorous benchmark data for first-principles theoretical methods, which is indispensable for the development of new methodologies to simulate extreme states of matter [4,5,33]. Finally, the detailed resolution of electronic features of different materials constitutes an important end in itself, and promises novel insights into the behavior of matter across various density and temperature regimes.

Experimental setup. The experiment was performed at the HED instrument [34] of the European XFEL, Germany. The XFEL beam was self-seeded to an energy of $E_0 \sim$ 7703 eV, and then passed through a four-bounce silicon (111) monochromator with an acceptance range of 0.8 eV to remove the underlying self-amplified spontaneous emission (SASE) pedestal from the beam. The beam was focused onto a 50 μm thick Al foil using a set of Be compound refractive lenses [34] located 9 m upstream to a spot of order 10 μm. The full width at half maximum (FWHM) of the beam incident on the sample was measured to be $\Delta E \sim 450$–530 meV, corresponding to a spectral bandwidth of $\Delta E/E \sim 5.8 - 6.9 \times 10^{-5}$, as measured from the quasielastic scattering feature. An upstream gas monitor measured initial beam energies of 146–310 μJ, however transmission through the beam line optics (∼70%) and after removal of the large SASE pedestal in the monochromator reduced the energy on target to 15.5–21.8 μJ (∼7% transmission), as measured on a second gas monitor before the target. Removing the SASE pedestal was critical in this experiment since the seeding performance was unsatisfactory and ∼85% of the fluence was not in the seed. Furthermore, due to the convolution of Eq. (1) the brighter and broader pedestal would blur our measured XRTS signal.

The scattered x-rays were collected by a spherically bent Si (533) diced crystal analyser (DCA) previously employed to measure phonons [19] and described in more detail by Ref. [26], and shown diagrammatically in Fig. 1. However, in contrast to Ref. [26] where scattering was measured in a spectral range of just 0.3 eV, here we measure the signal up to energy losses of 40 eV. The incident photons collected by the DCA are dispersed and focused onto a Jungfrau detector [35] employing asymmetric pixels, with a size of 25 μm in the dispersive direction and 225 μm in the nondispersive direction. The detector is single-photon sensitive with an excellent noise of 150 eV in the highest gain stage (or 0.02 photons at 7700 eV) [36]. Individual images can be thresholded to eliminate electronic noise and detect only single photon events giving a noise level well below the Poisson statistical noise for single photon detection events [36]. It is the combination of monochromating the incident beam and collection of the scattered photons on the ultrahigh resolution DCA spectrometer that allows for high fidelity measurements of the XRTS signal on electronic energy scales.

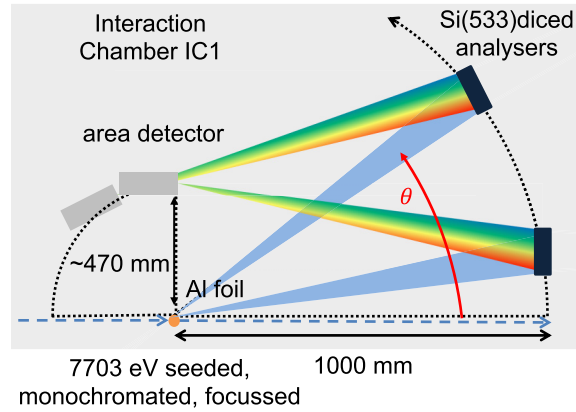

FIG. 1. Schematic illustration of the setup in Interaction Chamber 1 (IC1) modified from Wollenweber *et al.* [26]. The x-ray beam is seeded at 7703 eV in the SASE2 undulator including a SASE pedestal. The beam is passed through a four-bounce Si (111) monochromator to remove this SASE pedestal before being focused onto an Al foil. The x-rays are scattered, collected, and focused by a spherically bent diced analyzer crystal onto a Jungfrau detector with asymmetric pixels. Both the analyzer and detector are mounted onto curved rails to vary the scattering angle θ. The detector is shown in two configurations: at 13.6° corresponding to $(\pi/2 - \theta_B)$ the Bragg angle with the detector plane directly above the sample; and the highest angle. The scattering angle can be freely set between 3.6° and 25.6° in this study. The combination of the monochromated beam and ultrahigh resolution spectrometer allows for the high-fidelity measurements of electronic structure.

The primary source of uncertainty in the plasmon measurement is due to the finite angular coverage of the DCA. This results in so-called q broadening, where the inelastic signal measured is integrated over a range of scattering vectors. To narrow the angular coverage of the DCA, a horizontal slit mask made from Al was placed on the DCA, which reduced its coverage to ±1.4°, or a q range of $\pm 0.095\,\text{Å}^{-1}$ to $\pm 0.098\,\text{Å}^{-1}$. This slit width was chosen as a compromise between reducing the q broadening and maximizing the reflectivity of the DCA through the number of reflecting dice [26]. For our measurement the DCA has uniform reflectivity in our q window, and the calculated standard deviation of our q measurement is $\sim \pm\, 0.03\,\text{Å}^{-1}$.

The DCA reflects a spectral window of 3.5 eV at the Bragg angles used in this experiment, so it must be scanned in Bragg angle to collect spectra at different energies. To mitigate the drop off in reflectivity in the wings of the spectra [26], the DCA was conservatively scanned in small steps so that the spectral windows overlap. Relaxing this condition, the

plasmon feature could be collected in only two to three steps since the window is so wide, substantially reducing the number of shots required to collect the plasmon. An estimate of the SNR $= \sqrt{NI}$ (signal-to-noise ratio), where I is the integrated intensity in photons/shot and N the number of shots. We estimate that a total of 10^3–10^4 shots should be sufficient for a SNR $\sim$ 6–28 at the plasmon feature, which requires a collection time of <20 minutes at 10 Hz; fewer shots are required with higher flux. Better seeding performance could allow the omission of the monochromator, further increasing the intensities achieved at the sample.

The recorded spectral window was calibrated using Co K$_\beta$ emission and the position of the quasielastic scattering. This was established accurately by tuning the seeded beam energy to cross the Co K edge and observing when the intensity of the elastically scattered photons plateaued relative to the Co K-shell emission recorded by a spectrometer [37] viewing the upstream side of a Co foil. The incident photon beam was determined from this method to have a central photon energy of $E_0 = 7703.21$ eV for this study on Al, and the energy dispersion was determined to be 22.54 meV/pixel.

To measure the plasmon at a range of individual scattering vectors, the DCA setup was moved to different scattering angles between 3.6° and 25.6°, corresponding to $q = 0.245 - 1.730$ Å^{-1}. This allows the dynamic structure factor of Al to be probed from the collective regime up into the electron-hole pair continuum, cf. Fig. 3.

Results. In Fig. 2, we display the measured XRTS intensity as a function of the photon energy loss $E = E_0 - E_s$. The inset shows the quasielastic feature around $E = E_0$ corresponding to the combined source and instrument function $R(E_s)$; it is approximately Gaussian with a full width at half maximum of $\Delta E = 0.46$ eV ($\sigma = 0.2$ eV). The horizontal dashed lines indicate the zero intensity base lines for the five considered wave numbers $q \in [0.25, 1.73]$ Å^{-1}, and the corresponding intensities are shown as the colored curves. Remarkably, the effect of the convolution of $S_{ee}(q, E)$ with $R(E_s)$ [cf. Eq. (1)] can be neglected in practice due to the high resolution of our setup. At the same time, we are able to accurately resolve the plasmon down to below 20% of the Fermi wave number due to the high brilliance of the XFEL, and its excellent repetition rate. This remarkable performance might even open up new possibilities to connect XRTS with the estimation of optical properties such as the dielectric function, opacity, and electrical conductivity, which are defined for $q \to 0$ [32,39].

The resulting dispersion relation of aluminium is shown in Fig. 3, where we indicate our measurement of the plasmon position as a function of q. The finite size of the DCA covers a q range of $\sim \pm 0.1$ Å^{-1}: to be clear, this does not represent an uncertainty in central q value as the angular position of the DCA was initially measured and then carefully positioned using motors; instead, it represents the range of values of q over which the XRTS spectrum is averaged. As the number of die in the DCA is uniform in q, the q uncertainty plotted in Fig. 3 are the standard deviation for a uniform distribution, which gives an accuracy of $\sim \pm 0.03$ Å^{-1}, almost exactly the same as previous EELS measurements [29]. The accuracy in the plasmon shift is mainly due to the calibration of the energy axis, which is explained in more detail in the Supplemental Material [38]. Identified plasmon peaks are fitted with the expected quadratic dispersion relation of the form

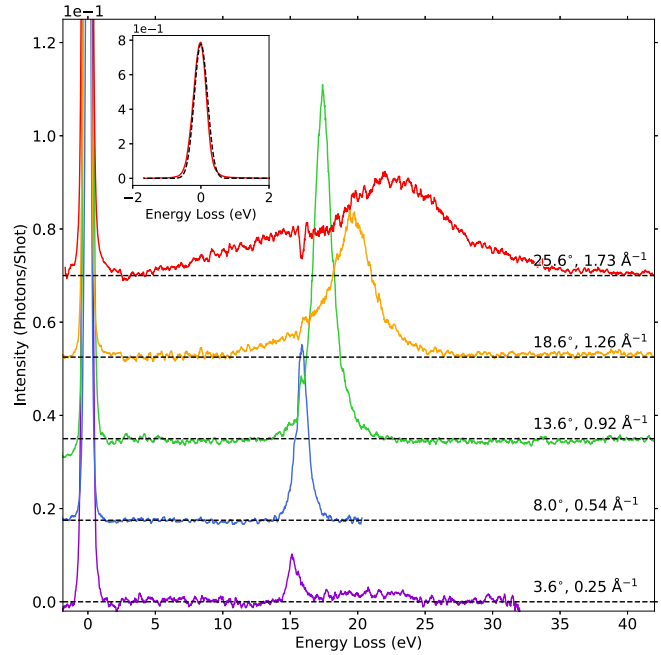

FIG. 2. Measured XRTS intensity for five different wave numbers as a function of the photon energy loss $E = E_0 - E_s$ in units of integrated intensity in photons/shot. The curves are offset vertically for clarity and show the variation in position, intensity, and shape of the plasmon in aluminium. Further details on the collection of the spectra are provided in the table in the Supplemental Material [38]. Inset: example spectrum of the narrow quasielastic scattering (red) for the highest wave number, and a Gaussian fit with $\sigma = 0.19$ eV (black dashed). The intensity of the quasielastic scattering uses the same scale as the main figure.

$$\omega = \omega_p + \alpha \frac{\hbar^2 q^2}{m_e}, \tag{2}$$

following the familiar Bohm-Gross relation [42], where $\hbar$ is the reduced Planck constant and m_e is the electron mass. We determine a prefactor of $\alpha = 0.370 \pm 0.003$ and plasma frequency of $\omega_p = 15.067 \pm 0.015$ eV where the error is the standard deviation calculated using the total least squares, accounting for the uncertainties in q and the plasmon shift. We find excellent agreement with previous EELS measurements [28,29], which further substantiates the high quality of our results, and indeed improves on the accuracy in the scaling parameter α. Above the electron-hole pair continuum [40], where the plasmon decays into a multitude of excitations due to Landau damping, the position of the maximum in $S_{ee}(q, E)$ deviates from Eq. (2), and the experimental spectrum attains a broad, nontrivial shape (see the curve in Fig. 2 for highest q).

Let us next utilize our new high-resolution XRTS data to assess the accuracy of *ab initio* time-dependent density functional theory (TDDFT) simulations [24,25,43]. As a first step, we carried out linear-response TDDFT calculations employing the adiabatic local density approximation (ALDA) for the four lowest q values; see the Supplemental Material [38] and references therein [29,37,44–53] for technical details. The corresponding peak positions only considering the central q

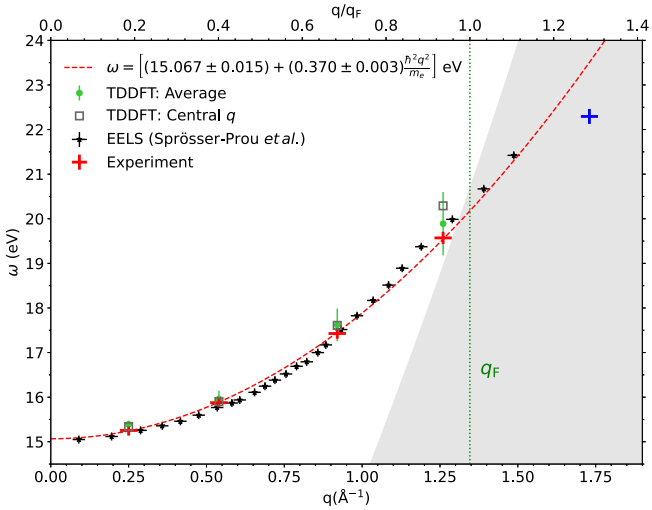

FIG. 3. Plasmon dispersion of aluminium. Crosses: experimental peak position and associated uncertainty, with red below the pair continuum, and blue in the pair continuum; red dashed line: the experimental data fitted to the dispersion of Eq. (2); black stars: previous EELS measurements of the Al plasmon by Sprösser-Prou *et al.* [29]; green circles: TDDFT average plasmon position, with the error bars indicating the standard deviation of the peak position in the q range; gray squares: TDDFT plasmon position only at the central q value. The shaded gray area indicates the pair continuum [40], and the dotted vertical line the Fermi wave number q_F in bulk Al with a face-centered cubic (fcc) lattice [41].

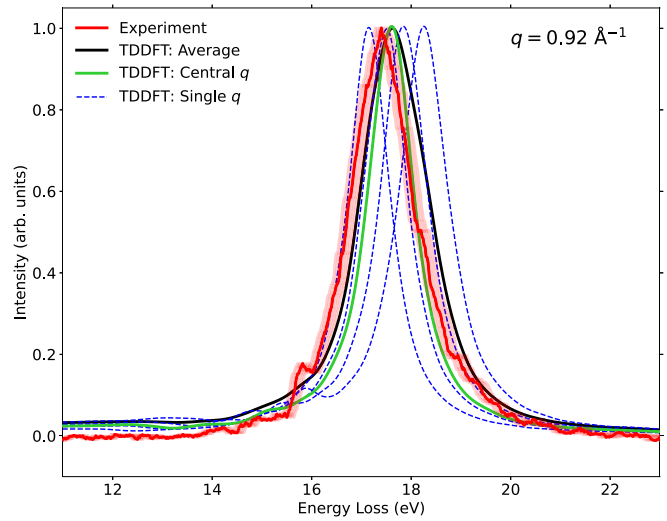

FIG. 4. Using high-resolution XRTS measurements (solid red) to benchmark first-principles TDDFT simulations at $q_0 = 0.92$ Å^{-1}. The solid green curve is from a single TDDFT simulation at $q_0 = 0.932$ Å^{-1}, the closest our simulation box size allows us to get to the central q value. The blue dashed curves have been obtained from single TDDFT simulations at different q values in the experimental range: 0.858, 0.914, 0.972, 1.029 Å^{-1}. The solid black line has been averaged over the five individual TDDFT results with equal weighting. The red area indicates the experimental uncertainty in the plasmon position.

are included in Fig. 3 and are in reasonable agreement with the experimental data points for the three smallest probed wave numbers, but significantly overestimate the true plasmon position for $q = 1.3$ Å^{-1}. To get additional insights into the quality of the TDDFT simulations, we show a detailed comparison of the latter with the experimental intensity in Fig. 4 for $q = 0.92$ Å^{-1}, clearly demonstrating that TDDFT underestimates the peak width despite reproducing the peak position with good accuracy.

While the attribution of such deviations between experiment and simulation to a systematic error due to the employed approximation for the exchange-correlation functional or exchange-correlation kernel is tempting, other explanations have to be considered. First, it is noted that the earlier XRTS experiments had substantially broader source-and-instrument functions [24], which might obscure the true origin of an observed deviation. The ultrahigh resolution achieved here resolves this conundrum and rules out any significant effects due to $R(E_s)$. Second, the finite angular coverage of the employed DCAs implies that the experimental spectra are effectively averaged over a finite interval of q values. To rigorously take into account this effect, we have carried out a series of TDDFT simulations for a uniformly distributed set of wave numbers $q \in [-\Delta q + q_0, \Delta q + q_0]$, and the results are included in Fig. 4 (single q). Interestingly, such slight changes in the wave number significantly affect the peak position, width, shape, and symmetry of the generated XRTS spectra. As our best prediction of the measured XRTS intensity, these generated spectra are averaged over the q range with equal weight [38], providing substantially improved agreement with the experimental observation both with respect to its form and position (see average in Fig. 4). While the TDDFT wings appear slightly higher than the measured curve, they are nevertheless within the experimental uncertainty in the intensity. The same holds for the other three considered wave numbers, which are shown in the Supplemental Material [38]. In this way, our setup has allowed observed differences between TDDFT simulations and XRTS experiments to be reconciled, which we attribute to the mixing of wave numbers for the present case. For completeness, we have included the properly q-averaged peak positions in Fig. 3 as well as an indication of the variance of the TDDFT results within the appropriate q window. The effect of averaging is small for $q \lesssim 1$ Å^{-1}, but leads to a substantial improvement for the second largest wave number: here the importance of averaging correctly over the q range is clearly demonstrated.

Conclusion. In this Letter, we have presented new ultrahigh resolution XRTS measurements of electronic features obtained at the European XFEL. Our setup works over a broad range of wave numbers and can be implemented in both forward and backward scattering geometries in future experiments. As a practical example, the plasmon in aluminium at ambient conditions was studied, which was resolved with high accuracy even at very small scattering angles. This opens up the enticing opportunity to connect XRTS measurements with the estimation of optical properties such as the electrical conductivity.

We are convinced that our work opens up a variety of possibilities for important future research. First, resolving the electronic structure of different materials with high resolution is important in its own right and will give new insights into

physical effects such as the predicted roton-type excitation in low-density hydrogen [54,55], or very recently reported thermal features in isochorically heated materials [41,56]. Recent performance on the SASE2 undulator [57] has demonstrated a spectral density of 1 mJ/eV in the seeded beam which would yield fluences of 10^{11} photons/pulse delivered at 10 Hz. Whilst comparable to synchrotrons, this high fluence can be delivered at femtosecond timescales (typical FWHM of 25 fs) and focused into a small volume yielding intensities per pulse $\sim 10^{17}$ W/cm^2, heating the electronic system faster than the electron-ion coupling time, which is more than sufficient to heat into the WDM regime [32]. In addition, the narrow width of $R(E_s)$ facilitates the rigorous benchmarking of theoretical models [58,59] and first-principles simulations [4,60] such as the exchange-correlation functional and exchange-correlation kernel in TDDFT calculations [24,25,61,62].

A particularly important field of application is given by the diagnosis of experiments with matter under extreme conditions. Specifically, a narrow source-and-instrument function is key to extend the model-free interpretation of XRTS spectra to temperatures of the order of $T \sim 1$ eV, whereas previous efforts were restricted to $T \gtrsim 10$ eV [20,21]. This development promises to unlock the full capability of modern XFEL facilities such as the European XFEL in Germany [27] and the Linac Coherent Light Source (LCLS) in the USA [63] to study matter at planetary interior conditions [7], to diagnose material science and material discovery applications, and to characterize states that occur on the initial stage of the compression path of the fuel capsule in inertial confinement fusion experiments.

Acknowledgments. We acknowledge the European XFEL in Schenefeld, Germany, for provision of X-ray free-electron laser beamtime at the Scientific Instrument HED (High Energy Density Science) under Proposal No. 3777 and would like to thank the staff for their assistance. The authors are grateful to the HIBEF user consortium for the provision of instrumentation and staff that enabled this experiment. The original datasets can be found here and are available upon reasonable request: doi:10.22003/XFEL.EU-DATA-003777-00.

This work was partially supported by the Center for Advanced Systems Understanding (CASUS) which is financed by Germany's Federal Ministry of Education and Research (BMBF) and by the Saxon state government out of the State budget approved by the Saxon State Parliament. This work has received funding from the European Union's Just Transition Fund (JTF) within the project *Röntgenlaser-Optimierung der Laserfusion* (ROLF), Contract No. 5086999001, cofinanced by the Saxon state government out of the State budget approved by the Saxon State Parliament. This work has received funding from the European Research Council (ERC) under the European Union's Horizon 2022 research and innovation programme (Grant Agreement No. 101076233, "PREXTREME"). Views and opinions expressed are however those of the authors only and do not necessarily reflect those of the European Union or the European Research Council Executive Agency. Neither the European Union nor the granting authority can be held responsible for them.

The TDDFT calculations were partly carried out at the Norddeutscher Verbund für Hoch- und Höchstleistungsrechnen (HLRN) under Grant No. mvp00024, and on a Bull Cluster at the Center for Information Services and High Performance Computing (ZIH) at Technische Universität Dresden.

[1] J. Sheffield, D. Froula, S. H. Glenzer, and N. C. Luhmann, *Plasma Scattering of Electromagnetic Radiation: Theory and Measurement Techniques* (Academic Press, 2010).

[2] S. H. Glenzer and R. Redmer, X-ray thomson scattering in high energy density plasmas, Rev. Mod. Phys. **81**, 1625 (2009).

[3] G. Gregori, S. H. Glenzer, W. Rozmus, R. W. Lee, and O. L. Landen, Theoretical model of x-ray scattering as a dense matter probe, Phys. Rev. E **67**, 026412 (2003).

[4] T. Dornheim, Z. A. Moldabekov, K. Ramakrishna, P. Tolias, A. D. Baczewski, D. Kraus, T. R. Preston, D. A. Chapman, M. P. Böhme, T. Döppner, F. Graziani, M. Bonitz, A. Cangi, and J. Vorberger, Electronic density response of warm dense matter, Phys. Plasmas **30**, 032705 (2023).

[5] F. Graziani, M. P. Desjarlais, R. Redmer, and S. B. Trickey (eds.), *Frontiers and Challenges in Warm Dense Matter* (Springer, International Publishing, 2014).

[6] R. P. Drake, *High-Energy-Density Physics: Foundation of Inertial Fusion and Experimental Astrophysics*, Graduate Texts in Physics (Springer Science & Business Media, 2006).

[7] A. Benuzzi-Mounaix, S. Mazevet, A. Ravasio, T. Vinci, A. Denoeud, M. Koenig, N. Amadou, E. Brambrink, F. Festa, A. Levy, M. Harmand, S. Brygoo, G. Huser, V. Recoules, J. Bouchet, G. Morard, F. Guyot, T. de Resseguier, K. Myanishi, N. Ozaki *et al.*, Progress in warm dense matter study with applications to planetology, Phys. Scr. **T161**, 014060 (2014).

[8] A. Becker, W. Lorenzen, J. J. Fortney, N. Nettelmann, M. Schöttler, and R. Redmer, Ab initio equations of state for hydrogen (h-reos.3) and helium (he-reos.3) and their implications for the interior of brown dwarfs, Astrophys. J. Suppl. Series **215**, 21 (2014).

[9] A. L. Kritcher, D. C. Swift, T. Döppner, B. Bachmann, L. X. Benedict, G. W. Collins, J. L. DuBois, F. Elsner, G. Fontaine, J. A. Gaffney, S. Hamel, A. Lazicki, W. R. Johnson, N. Kostinski, D. Kraus, M. J. MacDonald, B. Maddox, M. E. Martin, P. Neumayer, A. Nikroo *et al.*, A measurement of the equation of state of carbon envelopes of white dwarfs, Nature (London) **584**, 51 (2020).

[10] S. X. Hu, B. Militzer, V. N. Goncharov, and S. Skupsky, First-principles equation-of-state table of deuterium for inertial confinement fusion applications, Phys. Rev. B **84**, 224109 (2011).

[11] R. Betti and O. A. Hurricane, Inertial-confinement fusion with lasers, Nat. Phys. **12**, 435 (2016).

[12] D. Kraus, A. Ravasio, M. Gauthier, D. O. Gericke, J. Vorberger, S. Frydrych, J. Helfrich, L. B. Fletcher, G. Schaumann, B. Nagler, B. Barbrel, B. Bachmann, E. J. Gamboa, S. Göde, E. Granados, G. Gregori, H. J. Lee, P. Neumayer, W. Schumaker,

T. Döppner *et al.*, Nanosecond formation of diamond and lonsdaleite by shock compression of graphite, Nat. Commun. **7**, 10970 (2016).

[13] D. Kraus, J. Vorberger, A. Pak, N. J. Hartley, L. B. Fletcher, S. Frydrych, E. Galtier, E. J. Gamboa, D. O. Gericke, S. H. Glenzer, E. Granados, M. J. MacDonald, A. J. MacKinnon, E. E. McBride, I. Nam, P. Neumayer, M. Roth, A. M. Saunders, A. K. Schuster, P. Sun *et al.*, Formation of diamonds in laser-compressed hydrocarbons at planetary interior conditions, Nat. Astron. **1**, 606 (2017).

[14] A. Lazicki, D. McGonegle, J. R. Rygg, D. G. Braun, D. C. Swift, M. G. Gorman, R. F. Smith, P. G. Heighway, A. Higginbotham, M. J. Suggit, D. E. Fratanduono, F. Coppari, C. E. Wehrenberg, R. G. Kraus, D. Erskine, J. V. Bernier, J. M. McNaney, R. E. Rudd, G. W. Collins, J. H. Eggert *et al.*, Metastability of diamond ramp-compressed to 2 terapascals, Nature (London) **589**, 532 (2021).

[15] J. Vorberger, T. R. Preston, N. Medvedev, M. P. Böhme, Z. A. Moldabekov, D. Kraus, and T. Dornheim, Revealing non-equilibrium and relaxation in laser heated matter, Phys. Lett. A **499**, 129362 (2024).

[16] S. H. Glenzer, O. L. Landen, P. Neumayer, R. W. Lee, K. Widmann, S. W. Pollaine, R. J. Wallace, G. Gregori, A. Höll, T. Bornath, R. Thiele, V. Schwarz, W.-D. Kraeft, and R. Redmer, Observations of plasmons in warm dense matter, Phys. Rev. Lett. **98**, 065002 (2007).

[17] L. B. Fletcher, H. J. Lee, T. Döppner, E. Galtier, B. Nagler, P. Heimann, C. Fortmann, S. LePape, T. Ma, M. Millot, A. Pak, D. Turnbull, D. A. Chapman, D. O. Gericke, J. Vorberger, T. White, G. Gregori, M. Wei, B. Barbrel, R. W. Falcone *et al.*, Ultrabright x-ray laser scattering for dynamic warm dense matter physics, Nat. Photonics **9**, 274 (2015).

[18] S. Frydrych, J. Vorberger, N. J. Hartley, A. K. Schuster, K. Ramakrishna, A. M. Saunders, T. van Driel, R. W. Falcone, L. B. Fletcher, E. Galtier, E. J. Gamboa, S. H. Glenzer, E. Granados, M. J. MacDonald, A. J. MacKinnon, E. E. McBride, I. Nam, P. Neumayer, A. Pak, K. Voigt *et al.*, Demonstration of x-ray thomson scattering as diagnostics for miscibility in warm dense matter, Nat. Commun. **11**, 2620 (2020).

[19] A. Descamps, B. K. Ofori-Okai, K. Appel, V. Cerantola, A. Comley, J. H. Eggert, L. B. Fletcher, D. O. Gericke, S. Göde, O. Humphries, O. Karnbach, A. Lazicki, R. Loetzsch, D. McGonegle, C. A. J. Palmer, C. Plueckthun, T. R. Preston, R. Redmer, D. G. Senesky, C. Strohm *et al.*, An approach for the measurement of the bulk temperature of single crystal diamond using an x-ray free electron laser, Sci. Rep. **10**, 14564 (2020).

[20] T. Dornheim, M. P. Böhme, D. A. Chapman, D. Kraus, T. R. Preston, Z. A. Moldabekov, N. Schlünzen, A. Cangi, T. Döppner, and J. Vorberger, Imaginary-time correlation function thermometry: A new, high-accuracy and model-free temperature analysis technique for x-ray Thomson scattering data, Phys. Plasmas **30**, 042707 (2023).

[21] T. Dornheim, M. Böhme, D. Kraus, T. Döppner, T. R. Preston, Z. A. Moldabekov, and J. Vorberger, Accurate temperature diagnostics for matter under extreme conditions, Nat. Commun. **13**, 7911 (2022).

[22] K. Falk, E. J. Gamboa, G. Kagan, D. S. Montgomery, B. Srinivasan, P. Tzeferacos, and J. F. Benage, Equation of state measurements of warm dense carbon using laser-driven shock and release technique, Phys. Rev. Lett. **112**, 155003 (2014).

[23] T. Döppner, M. Bethkenhagen, D. Kraus, P. Neumayer, D. A. Chapman, B. Bachmann, R. A. Baggott, M. P. Böhme, L. Divol, R. W. Falcone, L. B. Fletcher, O. L. Landen, M. J. MacDonald, A. M. Saunders, M. Schörner, P. A. Sterne, J. Vorberger, B. B. L. Witte, A. Yi, R. Redmer *et al.*, Observing the onset of pressure-driven k-shell delocalization, Nature (London) (2023).

[24] M. Cazzaniga, Hans-Christian Weissker, S. Huotari, T. Pylkkänen, P. Salvestrini, G. Monaco, G. Onida, and L. Reining, Dynamical response function in sodium and aluminum from time-dependent density-functional theory, Phys. Rev. B **84**, 075109 (2011).

[25] K. Ramakrishna, A. Cangi, T. Dornheim, A. Baczewski, and J. Vorberger, First-principles modeling of plasmons in aluminum under ambient and extreme conditions, Phys. Rev. B **103**, 125118 (2021).

[26] L. Wollenweber, T. R. Preston, A. Descamps, V. Cerantola, A. Comley, J. H. Eggert, L. B. Fletcher, G. Geloni, D. O. Gericke, S. H. Glenzer, S. Göde, J. Hastings, O. S. Humphries, A. Jenei, O. Karnbach, Z. Konopkova, R. Loetzsch, B. Marx-Glowna, E. E. McBride, D. McGonegle *et al.*, High-resolution inelastic x-ray scattering at the high energy density scientific instrument at the european x-ray free-electron laser, Rev. Sci. Instrum. **92**, 013101 (2021).

[27] T. Tschentscher, C. Bressler, J. Grünert, A. Madsen, A. P. Mancuso, M. Meyer, A. Scherz, H. Sinn, and U. Zastrau, Photon beam transport and scientific instruments at the european XFEL, Appl. Sci. **7**, 592 (2017).

[28] K. J. Krane, Dispersion and damping of volume plasmons in polycrystalline aluminium and indium, J. Phys. F **8**, 2133 (1978).

[29] J Sprösser-Prou, A vom Felde, and J Fink, Aluminum bulk-plasmon dispersion and its anisotropy, Phys. Rev. B **40**, 5799 (1989).

[30] E. Runge and E. K. U. Gross, Density-functional theory for time-dependent systems, Phys. Rev. Lett. **52**, 997 (1984).

[31] R. Brydson, *Electron Energy Loss Spectroscopy* (Garland Science, 2020).

[32] B. B. L. Witte, L. B. Fletcher, E. Galtier, E. Gamboa, H. J. Lee, U. Zastrau, R. Redmer, S. H. Glenzer, and P. Sperling, Warm dense matter demonstrating non-drude conductivity from observations of nonlinear plasmon damping, Phys. Rev. Lett. **118**, 225001 (2017).

[33] M. Bonitz, T. Dornheim, Zh. A. Moldabekov, S. Zhang, P. Hamann, H. Kählert, A. Filinov, K. Ramakrishna, and J. Vorberger, Ab initio simulation of warm dense matter, Phys. Plasmas **27**, 042710 (2020).

[34] U. Zastrau, K. Appel, C. Baehtz, O. Baehr, L. Batchelor, A. Berghäuser, M. Banjafar, E. Brambrink, V. Cerantola, Thomas E Cowan, H. Damker, S. Dietrich, S. Di Dio Cafiso, Jörn Dreyer, Hans-Olaf Engel, T. Feldmann, S. Findeisen, M. Foese, D. Fulla-Marsa, S. Göde *et al.*, The high energy density scientific instrument at the European XFEL, J. Synchrotron Radiat. **28**, 1393 (2021).

[35] A. Mozzanica, M. Andrä, R. Barten, A. Bergamaschi, S. Chiriotti, M. Brückner, R. Dinapoli, E. Fröjdh, D. Greiffenberg, F. Leonarski, C. Lopez-Cuenca, D. Mezza, S. Redford, C. Ruder, B. Schmitt, X. Shi, D. Thattil, G. Tinti, S. Vetter, and J. Zhang, The JUNGFRAU detector for applications at synchrotron light sources and XFELs, Synchrotron Radiation News **31**, 16 (2018).

[36] A. Mozzanica, A. Bergamaschi, M. Brueckner, S. Cartier, R. Dinapoli, D. Greiffenberg, J. Jungmann-Smith, D. Maliakal, D. Mezza, M. Ramilli, C. Ruder, L. Schaedler, B. Schmitt, X. Shi, and G. Tinti, Characterization results of the JUNGFRAU full scale readout ASIC, J. Instrum. **11**, C02047 (2016).

[37] T. R. Preston, S. Göde, J.-P. Schwinkendorf, K. Appel, E. Brambrink, V. Cerantola, H. Höppner, M. Makita, A. Pelka, C. Prescher, K. Sukharnikov, A. Schmidt, I. Thorpe, T. Toncian, A. Amouretti, D. Chekrygina, R. W. Falcone, K. Falk, L. B. Fletcher, E. Galtier *et al.*, Design and performance characterisation of the HAPG von Hámos Spectrometer at the High Energy Density Instrument of the European XFEL, J. Instrum. **15**, P11033 (2020).

[38] See Supplemental Material http://link.aps.org/supplemental/10.1103/PhysRevB.109.L241112 for additional details on the experimental details, simulations, and wave number averaging.

[39] P. Sperling, E. J. Gamboa, H. J. Lee, H. K. Chung, E. Galtier, Y. Omarbakiyeva, H. Reinholz, G. Röpke, U. Zastrau, J. Hastings, L. B. Fletcher, and S. H. Glenzer, Free-electron x-ray laser measurements of collisional-damped plasmons in isochorically heated warm dense matter, Phys. Rev. Lett. **115**, 115001 (2015).

[40] G. Giuliani and G. Vignale, *Quantum Theory of the Electron Liquid* (Cambridge University Press, Cambridge, 2008).

[41] Z. A. Moldabekov, T. D. Gawne, S. Schwalbe, T. R. Preston, J. Vorberger, and T. Dornheim, Excitation signatures of isochorically heated electrons in solids at finite wavenumber explored from first principles, Phys. Rev. Res. **6**, 023219 (2024).

[42] D. Bohm and E. P. Gross, Theory of plasma oscillations. a. origin of medium-like behavior, Phys. Rev. **75**, 1851 (1949).

[43] C. Ullrich, *Time-Dependent Density-Functional Theory: Concepts and Applications*, Oxford Graduate Texts (Oxford University Press, Oxford, 2012).

[44] A. Savitzky and M. J. E. Golay, Smoothing and differentiation of data by simplified least squares procedures. Anal. Chem. **36**, 1627 (1964).

[45] P. Virtanen, R. Gommers, T. E. Oliphant, M. Haberland, T. Reddy, D. Cournapeau, E. Burovski, P. Peterson, W. Weckesser, J. Bright, S. J. van der Walt, M. Brett, J. Wilson, K. J. Millman, N. Mayorov, A. R. J. Nelson, E. Jones, R. Kern, E. Larson, C. J. Carey *et al.*, SciPy 1.0: Fundamental algorithms for scientific computing in python, Nature Methods **17**, 261 (2020).

[46] J. J. Mortensen, L. B. Hansen, and K. W. Jacobsen, Real-space grid implementation of the projector augmented wave method, Phys. Rev. B **71**, 035109 (2005).

[47] J. Enkovaara, C. Rostgaard, J. J. Mortensen, J. Chen, M. Dułak, L. Ferrighi, J. Gavnholt, C. Glinsvad, V. Haikola, H. A. Hansen, H. H. Kristoffersen, M. Kuisma, A. H. Larsen, L. Lehtovaara, M. Ljungberg, O. Lopez-Acevedo, P. G. Moses, J. Ojanen, T. Olsen, V. Petzold *et al.*, Electronic structure calculations with GPAW: A real-space implementation of the projector augmented-wave method, J. Phys.: Condens. Matter **22**, 253202 (2010).

[48] M. Walter, H. Häkkinen, L. Lehtovaara, M. Puska, J. Enkovaara, C. Rostgaard, and J. J. Mortensen, Time-dependent density-functional theory in the projector augmented-wave method, J. Chem. Phys. **128**, 244101 (2008).

[49] J. Yan, J. J. Mortensen, K. W. Jacobsen, and K. S. Thygesen, Linear density response function in the projector augmented wave method: Applications to solids, surfaces, and interfaces, Phys. Rev. B **83**, 245122 (2011).

[50] A. H. Larsen, J. J. Mortensen, J. Blomqvist, I. E. Castelli, R. Christensen, M. Dułak, J. Friis, M. N. Groves, B. Hammer, C. Hargus, E. D. Hermes, P. C. Jennings, P. B. Jensen, J. Kermode, J. R. Kitchin, E. L. Kolsbjerg, J. Kubal, K. Kaasbjerg, S. Lysgaard, J. B. Maronsson *et al.*, The atomic simulation environment–a Python library for working with atoms, J. Phys.: Condens. Matter **29**, 273002 (2017).

[51] S. R. Bahn and K. W. Jacobsen, An object-oriented scripting interface to a legacy electronic structure code, Comput. Sci. Eng. **4**, 56 (2002).

[52] R. W. G Wyckoff, *Crystal Structures* (Interscience Publishers, New York, 1948).

[53] J. P. Perdew and Y. Wang, Accurate and simple analytic representation of the electron-gas correlation energy, Phys. Rev. B **45**, 13244 (1992).

[54] P. Hamann, L. Kordts, A. Filinov, M. Bonitz, T. Dornheim, and J. Vorberger, Prediction of a roton-type feature in warm dense hydrogen, Phys. Rev. Res. **5**, 033039 (2023).

[55] T. Dornheim, Z. Moldabekov, J. Vorberger, H. Kählert, and M. Bonitz, Electronic pair alignment and roton feature in the warm dense electron gas, Commun. Phys. **5**, 304 (2022).

[56] Z. Moldabekov, T. D. Gawne, S. Schwalbe, T. R. Preston, J. Vorberger, and T. Dornheim, Ultrafast heating induced suppression of d-band dominance in the electronic excitation spectrum of cuprum, ACS Omega (2024), doi:10.1021/acsomega.4c02920.

[57] S. Liu, C. Grech, M. Guetg, S. Karabekyan, V. Kocharyan, N. Kujala, C. Lechner, T. Long, N. Mirian, W. Qin, S. Serkez, S. Tomin, J. Yan, S. Abeghyan, J. Anton, V. Blank, U. Boesenberg, F. Brinker, Y. Chen, W. Decking *et al.*, Cascaded hard X-ray self-seeded free-electron laser at megahertz repetition rate, Nat. Photonics **17**, 984 (2023).

[58] C. Mo, Z.-G. Fu, P. Zhang, W. Kang, W. Zhang, and X. T. He, First-principles method for x-ray thomson scattering including both elastic and inelastic features in warm dense matter, Phys. Rev. B **102**, 195127 (2020).

[59] Y. Zhang, C. Mo, P. Zhang, and W. Kang, A composite ansatz for calculation of dynamical structure factor, Chin. Phys. Lett. **41**, 017801 (2024).

[60] A. D. Baczewski, L. Shulenburger, M. P. Desjarlais, S. B. Hansen, and R. J. Magyar, X-ray thomson scattering in warm dense matter without the chihara decomposition, Phys. Rev. Lett. **116**, 115004 (2016).

[61] Z. Moldabekov, M. Böhme, J. Vorberger, D. Blaschke, and T. Dornheim, *Ab Initio* static exchange–correlation kernel across Jacob's Ladder without functional derivatives, J. Chem. Theory Comput. **19**, 1286 (2023).

[62] M. Schörner, M. Bethkenhagen, T. Döppner, D. Kraus, L. B. Fletcher, S. H. Glenzer, and R. Redmer, X-ray thomson scattering spectra from density functional theory molecular dynamics simulations based on a modified chihara formula, Phys. Rev. E **107**, 065207 (2023).

[63] C. Bostedt, S. Boutet, D. M. Fritz, Z. Huang, H. Ja Lee, H. T. Lemke, A. Robert, W. F. Schlotter, J. J. Turner, and G. J. Williams, Linac coherent light source: The first five years, Rev. Mod. Phys. **88**, 015007 (2016).